Pyrrolidium- and Imidazolium-Based Ionic Liquids and Electrolytes with Flexible Oligoether Anions

ChemPhysChem

Research Article
doi.org/10.1002/cphc.202300810

Chemistry Europe
European Chemical Societies Publishing

www.chemphyschem.org

Pyrrolidium- and Imidazolium-Based Ionic Liquids and Electrolytes with Flexible Oligoether Anions

Mukhtiar Ahmed,[a] Andrei Filippov,[a] Patrik Johansson,*[b] and Faiz Ullah Shah*[a]

A new class of fluorine-free ionic liquids (ILs) and electrolytes based on aliphatic flexible oligoether anions, 2-(2-methoxyethoxy)acetate (MEA) and 2-[2-(2-methoxyethoxy)ethoxy]-acetate (MEEA), coupled with pyrrolidinium and imidazolium cations is introduced. For the ILs with MEEA anions, Li^+ conducting electrolytes are created by doping the ILs with 30 mol% of LiMEEA. The structural flexibility of the oligoether functionality in the anion results in glass transition temperatures (T_g) as low as −60 °C for the neat ILs and the electrolytes. The imidazolium-based ILs and electrolytes reveal better thermal stabilities but higher T_g and lower electrochemical stabilities than the corresponding pyrrolidinium-based analogues. All neat ILs show comparable transport properties for the cations and these decrease by the addition of lithium salt – the pyrrolidinium-based electrolyte being affected the most.

Introduction

The liquid electrolytes used in conventional lithium-ion batteries (LIBs) are made by dissolving lithium hexafluorophosphate ($LiPF_6$) in flammable organic solvents such as ethylene carbonate (EC) mixed with linear carbonates, where EC facilitates Li^+ solvation and the formation of a stable solid electrolyte interphase (SEI) on the graphite anode,[1,2] while the linear carbonates, such as dimethyl carbonate (DMC), diethyl carbonate (DEC), and/or ethyl methyl carbonate (EMC), improve the physical, especially reduces viscosity, and electrochemical characteristics.[3,4] These linear carbonates, however, have low flash points and can easily catch fire in batteries under severe conditions, and this can in turn result in catastrophic thermal runaway.[5]

Another main concern with conventional organic liquid electrolytes is the $LiPF_6$ salt, which has been proven to decompose at elevated temperatures producing PF_5 and LiF, the former rapidly reacting with traces of water releasing highly toxic hydrofluoric acid (HF) and a reactive intermediate phosphoryl fluoride (POF_3),[6] which is even more toxic than HF. These decomposition products are also extremely reactive towards both cathodes and anodes, adversely affecting the performance and service life of a battery[7,8] and creating enormous health and environmental problems during the battery recycling process.[9] Taken altogether, it is imperative that the current organic liquid electrolytes are replaced by non-flammable, fluorine-free, and yet performant electrolytes.

Oligoethers (also known as "glymes") are a group of organic compounds with the general chemical formula [R-$(OCH_2CH_2)_n$-OR], often referred to by the abbreviation G*n*, where "*n*" stands for the number of repeating units and indicated by the letters monoglyme (G1), diglyme (G2), triglyme (G3), tetraglyme (G4), *etc.* This class of solvents has been intensively examined during the past two decades, mostly because of their attractive physicochemical features.[10–12] Glymes can even dissolve an equimolar amount of some lithium salts *via* an ether multidentate coordination functionality, making complexes known as solvate ionic liquids (SILs) as they mimic ionic liquids (ILs), with high thermal and electrochemical stabilities.[13] The Lewis acidity of Li^+ is substantially decreased as a result of the complex formation, which is equivalent to the production of weakly Lewis-basic anions such as PF_6^- and BF_4^- with the interaction of a Lewis acid.[14] Compared to carbonate-based organic solvents, glymes have higher flash points and better solubility of lithium salts,[15] but due to the presence of oxygen lone pairs they suffer from instability at high redox potentials.[16]

This work is a continuation of our previous study of phosphonium-based ILs with oligoether-based anions.[10] The main objectives of this study is to combine the oligoether-based anions with pyrrolidinium and imidazolium cations and investigate the effects of cation structures on the Li-salt solubility, thermal and electrochemical stabilities, and ion transport properties of the resulting ionic liquids and electrolytes. In addition, we here exploit the characteristics of glyme solvents with those of ILs based on small organic cations such as pyrrolidinium and imidazolium. Undoubtedly, electrolytes based on ILs offer a range of suitable advantages including low volatility and high thermal and electrochemical stabilities and can additionally be made fluorine-free and task-specific with synthetic diversity.[17–19] In general, their physicochemical and transport properties are determined by the sizes of ions and the

[a] *M. Ahmed, A. Filippov, F. U. Shah*
Chemistry of Interfaces, Luleå University of Technology,
SE-971 87 Luleå, Sweden
E-mail: faiz.ullah@ltu.se

[b] *P. Johansson*
Materials Physics, Department of Physics,
Chalmers University of Technology,
SE-412 96 Gothenburg, Sweden
E-mail: patrik.johansson@chalmers.se

Supporting information for this article is available on the WWW under https://doi.org/10.1002/cphc.202300810

interactions between the cations and anions, which can be functionalized due to the vast freedom in structural design to reduce these interactions and enhance the ion mobilities.[20–23]

Experimental

Materials and Synthesis

Unless otherwise stated, all the commercial reagents were utilized without any additional purification. 1,2-dimethylimidazole (ACS reagents, >97% purity), *n*-methylpyrrolidine (ACS reagents, >97% purity), 1-bromobutane (>99% purity), silver(I) oxide (>99.9% purity), 2-[2-(2-methoxyethoxy)ethoxy]acetic acid (>97% purity), 2-(2-methoxyethoxy)acetic acid (>97% purity) and lithium hydroxide monohydrate (ACS reagents, >98% purity) were received from Sigma–Aldrich. Sodium sulphate, dichloromethane (DCM) and diethyl ether were purchased from VWR (BDH) chemicals. The synthesis and structural characterization of the ILs are detailed in the supporting information (SI).

The electrolytes were made by dissolving 30 mol% of the corresponding lithium salts in the neat ILs to get concentrated solutions. All the samples were kept in a vacuum oven at 80 °C for at least four days before any measurement. The water content was measured by Karl Fischer titration (using Metrohm 917 Coulometer, Switzerland) placed inside an argon filled Mbraun glovebox and was determined to be less than 100 ppm for all synthesized ILs and the electrolytes (Table 1).

Nuclear Magnetic Resonance Spectroscopy

The structures and purity of all the synthesized products were confirmed by using a Bruker Ascend Aeon WB 400 (Bruker BioSpin AG, Fallanden, Switzerland) nuclear magnetic resonance (NMR) spectrometer. $CDCl_3$ was used as a solvent. The working frequencies were 400.21 MHz for ^{1}H, 100.64 MHz for ^{13}C, and 162.01 MHz for ^{31}P. Data were processed using the Bruker Topspin 3.5 software.

Thermal Analysis

Thermogravimetric analysis (TGA) was performed using a PerkinElmer TGA 8000 under N_2 gas at a heating rate of 10 °C per min. About 2–4 mg of sample was used for each experiment. The onset temperature of decomposition, T_{onset}, was calculated from the intersection of the baseline weight and the tangent of the weight versus temperature curve using the Pyris software. Differential scanning calorimetry (DSC) was performed using a PerkinElmer DSC 6000 on 2–5 mg of sample placed in an aluminium pan. DSC data were collected at a scanning rate of 5 °C min^{-1} for both cooling and heating traces. To maintain an inert environment inside the sample chamber, dry N_2 gas was delivered at a constant flow rate of 20 mL min^{-1}. The glass transition temperature (T_g) was determined by using the inflection mid-point of the initial *S*-shaped transition slope and determined from the *onset* with the help of the Pyris software.

Electrochemical Characterization

The electrochemical stability and ionic conductivity were determined using a Metrohm Autolab PGSTAT302N electrochemical workstation with a FRA32 M module for impedance measurements, all controlled by the Nova 2.02 software. A sealed Microcell HC from rhd instruments Germany was used to hold about 70 μL of the liquid sample. To determine the electrochemical stability window (ESW), linear sweep voltammetry (LSV) and cyclic voltammetry (CV) were performed with a three-electrode setup: a glassy carbon (GC) wire as working electrode (WE), a Pt crucible as counter electrode (CE) as well as sample container, and an Ag wire coated with AgCl as pseudo-reference electrode (RE). Both cathodic and anodic scans were recorded at a rate of 1 mV s^{-1}. The electrochemical potentials were calibrated using ferrocene (Fc) as an internal reference and shifted using $E_{Li/Li^+} \approx E_{Fc/Fc^+} + 3.2$ V.[24] The ESWs limits were defined by a 0.1 mA cm^{-2} cut-off current density.

The ionic conductivity was obtained from the impedance measurements performed in a frequency range from 1 Hz to 1 MHz with an AC voltage amplitude of 10 mV_{rms}. All the impedance spectra were measured during heating and cooling over a temperature range from −20 to 100 ± 0.1 °C. A two-electrode configuration was employed for ionic conductivity measurements, with a wire GC as WE and a 70 μL Pt crucible as sample container as well as CE.

Prior to each CV and ionic conductivity measurement, both electrodes were polished with a Kemet diamond paste (0.25 μm). The cell constant was calculated using a Metrohm 100 S cm^{-1} KCl standard solution (K_{cell} = 18.5396 cm^{-1}). The cell was thermally equilibrated for 10 minutes before recording the impedance spectra.

PFG NMR Diffusometry

Pulsed field gradient (PFG) NMR diffusometry measurements were performed using a Bruker Ascend/Aeon WB 400 (Bruker BioSpin AG) NMR spectrometer with a resonance frequency of 400.27 MHz for ^{1}H and 155.56 MHz for ^{7}Li. The PFG NMR measurements were performed with a PFG NMR probe Diff50 (Bruker) with a maximum amplitude of the magnetic field gradient pulse of 29.73 T m^{-1}. The samples were placed in a standard 5 mm NMR glass tube and

Table 1. Physiochemical properties of the ILs and the electrolytes.

System	Water content (ppm)	T_g (°C)	T_d (°C)	σ (S cm^{-1}) @ 20 °C	E_C (vs Li/Li^+)	E_A (vs Li/Li^+)	ESW
(MBPyrr)(MEA)	<71	−79	200	—	—	—	—
(MBPyrr)(MEEA)	<69	−77	207	4.2×10^{-4}	0.60	4.05	3.45
(MMBIm)(MEA)	<79	−72	211	3.3×10^{-4}	1.25	4.26	3.01
(MMBIm)(MEEA)	<74	−63	235	4.6×10^{-4}	0.73	4.14	3.41
$[(MBPyrr)(MEEA)]_{0.7}$ $[Li(MEEA)]_{0.3}$	<89	−69	231	7.5×10^{-5}	0.47	4.07	3.60
$[(MMBIm)(MEEA)]_{0.7}$ $[Li(MEEA)]_{0.3}$	<92	−61	245	8.4×10^{-5}	1.50	4.36	2.86

closed with a plastic stopper to avoid contact with air. Prior to measurements, each sample was equilibrated at a specific temperature for 30 min. The details of the PFG NMR technique for measuring molecular diffusion coefficients are available elsewhere.[25] The diffusivity of a molecule is the diffusion decay (DD) of amplitude A of NMR spectral line, obtained by Fourier transformation of a descending half of stimulated-echo (StE), as a function of the amplitude of applied pulsed field gradient. For the stimulated echo pulse sequence used, DD of A in the case of simple non-associating molecular liquid can be described by the Eq. (1):[26]

$$A(g,\delta,t_d) = A(0)\exp(-\gamma^2 g^2 \delta^2 D t_d) \quad (1)$$

where $A(0)$ is the factor proportional to the proton content in the system, and to spin-lattice and spin-spin relaxation times, γ is the gyromagnetic ratio for a used nucleus; g and δ are the amplitude and duration of the gradient pulse; t_d is the diffusion time; and D is the self-diffusion coefficient. t_d was in the range 4–100 ms for ^{1}H diffusion and 5–15 ms for ^{7}Li diffusion. No diffusion time dependence was observed in these measurements.

Results and Discussion

We start with the synthesis and structural characterization of the neat ILs and the electrolytes, followed by investigation of their thermal and phase behaviour before moving on to more battery-related properties such as electrochemical stability, ion transport properties including ionic conductivity, ion diffusivity and apparent transference numbers. Finally, variable temperature ^{7}Li NMR spectroscopy is employed to understand the Li^+ coordination and ion-ion interactions.

Synthesis and Characterization

A multistep protocol was used to synthesize the new oligoether functionalized ILs. The synthesis and characterization are briefly described here while the details are presented in the SI. The synthesis started with the preparation of the bromide salts,[27] which subsequently were converted into the corresponding hydroxides[28] using Ag_2O as an oxidizing agent and water as a solvent and hydroxy precursor at ambient temperature (Scheme S1). The hydroxide salts were further converted into ILs by a direct neutralization reaction with oligoether-based carboxylic acids in aqueous medium. The water was removed, and the products were dried prior to characterization.

The chemical structures of all the ILs agree well with the ^{1}H and ^{13}C NMR spectroscopic data. First, the ^{1}H NMR spectra of the ILs (Figures S1–S4) show characteristic resonance lines for the butyl chain, a triplet for the methylene protons alpha to the charged nitrogen atom appears in the range from 4.1 to 4.5 ppm for imidazolium and from 3.5 to 3.7 ppm for pyrrolidinium salts, and the doublet of three methyl protons with a distinct triplet appear around 0.9 ppm for both systems. Second, the ^{1}H resonance lines in the range from 3.5 to 4.3 ppm are attributed to the methylene protons of the ether chain in the anion and additionally the absence of any broad peak above 7 ppm confirm the deprotonation of the acids-anion formation, complimented by the presence of the aromatic signals at *ca.* 7.32 and 7.65 ppm for the imidazolium cation and verify the formation of the ILs. Finally, the presence of ^{13}C resonance lines in the ^{13}C NMR spectra around 65–72 ppm for ethoxy group, the appearance of signals at *ca.* 175 ppm for the carboxylate groups and the presence of ^{13}C resonance lines below 40 ppm for the aliphatic carbons (Figures S5–S8) confirm the successful synthesis of the targeted ILs. The structures and abbreviations of the synthesized ILs are shown in Figure 1.

Thermal properties

All the neat ILs show dynamic thermal stability $>200\,^{\circ}C$ as revealed by the TGA (Figure 2a and Table 1), which is considerably higher as compared with traditional organic liquid electrolytes.[29] To truly establish any long-term thermal stability of IL-based electrolytes, however, the dynamic TGA should be complemented by isothermal TGA.[30,31] It is clear that by

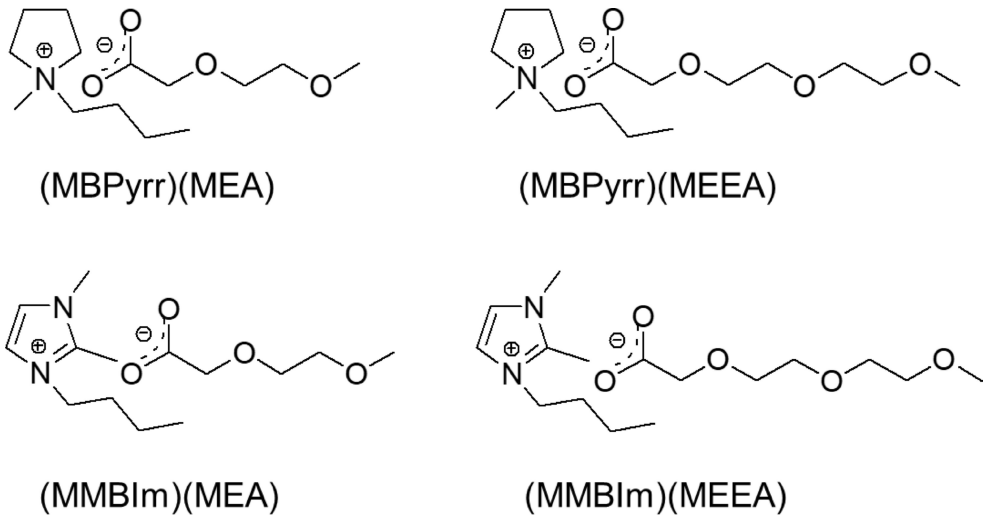

Figure 1. Chemical structures and abbreviations of the ILs and the ions.

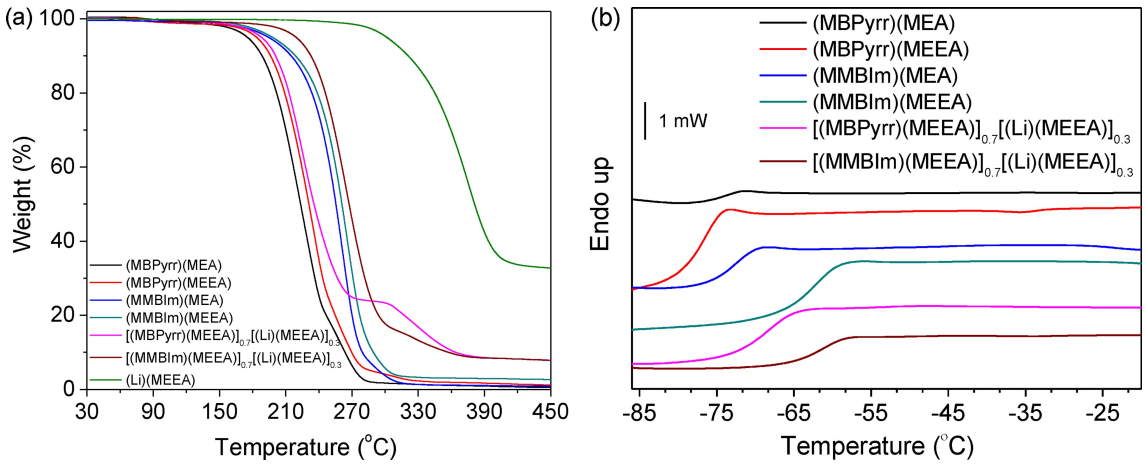

Figure 2. TGA thermograms of neat ILs and electrolytes (a), and DSC traces for neat ILs and electrolytes (b). The DSC traces in (b) are shifted along the Y-axis for clarity.

keeping the anion constant, the thermal decomposition of the imidazolium ILs proceed over a wider temperature region than for the pyrrolidinium analogues, suggesting the imidazolium ring to limit the thermal stability, which is consistent with the literature.[32,33] Keeping the cation constant, the IL with the bulkier oligoether anion is somewhat more stable, which is in contrast to observations made for ILs with oligoether cations.[34] This can be attributed to the oxygen electronegativity in the ether chain, which in cations weakens the covalent bond between the positively charged "*hetero*" atom and the alpha carbon, favouring thermal breakdown, while in the case of the anion it rather stabilizes the negative charge and somehow prevents the thermally induced decomposition.

As expected, and observed earlier,[10] the thermal stability of the LiMEEA salt is *ca.* 50 K higher than that of the neat ILs, which is due to the stronger electrostatic interactions and the absence of any organic cation; and for the same reasons, the thermal stability of the electrolytes is improved as compared to the parent ILs. Overall, thermal stability of neat ILs and electrolytes are slightly lower when compared to their phosphonium analogues.[10]

The corresponding DSC traces reveal that all the neat ILs and the electrolytes are glass-forming liquids, that is, they all exhibit glass transitions temperature (T_g), in the temperature range from −78 °C to −61 °C (Figure 2b and Table 1). The ethoxy groups of the anions are playing a decisive role in suppressing the crystallization of these salts. The imidazolium-based ILs exhibit higher T_g temperatures than the corresponding pyrrolidinium-based analogues, which might be due to the stronger ion-ion interactions mainly induced by the π-π stacking of the imidazolium rings,[35] and thus, a higher thermal energy is required to reach the same ionic mobility as for the pyrrolidinium-based ILs. For the same cation, increasing the number of ethylene oxide units in the anion increased the T_g, indicating a reduced mobility of the alkoxy chains. This agrees with the previous observations for ILs containing ether functionalized cations.[36,37] Doping of the ILs with 30 mol% LiMEEA salts slightly increased the T_g, which is quite expected due to the enhanced ionic interactions.[38,39]

Ionic Conductivity

Despite the structural differences, ionic conductivities of all the neat ILs are comparable throughout the whole studied temperature range and continuous increases are observed as a function of temperature (Figure 3). As compared to neat ILs, the electrolytes display lower ionic conductivities due to the decrease in free volume as a result of increased Coulombic interactions between the Li^+ ions and the anions, leading to aggregate formation. A similar trend has been observed for Li-salt doped ether functionalized ammonium-based[40] and phosphonium-based[10] ILs. Electrolytes with the imidazolium-based cations have higher ionic conductivities at lower temperature, but the difference diminishes at higher temperatures, mainly from increased concentration of charge carriers.[41]

The ionic conductivities are further analyzed by fitting the data to the following Vogel–Fulcher–Tammann (VFT) equation.[42]

$$\sigma = \sigma_0 \exp\left(\frac{-B}{(T - T_0)}\right) \quad (2)$$

Where σ_0 is a pre-exponential factor, B is an empirical material-dependent fitting parameter related to the T_g and activation/pseudo activation energy (E_σ) of the system. The reference temperature T_0 is attributed to the ideal vitreous transition temperature at which configurational entropy vanishes.[43] T_0 is determined by fitting the temperature-dependent ionic conductivity data to the VFT equation for the best linearity relationship. The resulting VFT parameters shows that E_σ for the imidazolium-based IL and their electrolytes is slightly higher than for the pyrrolidinium-based analogues, and even higher for electrolytes, indicating that the addition of Li-salts increases the ionic interactions, which agrees with the DSC data

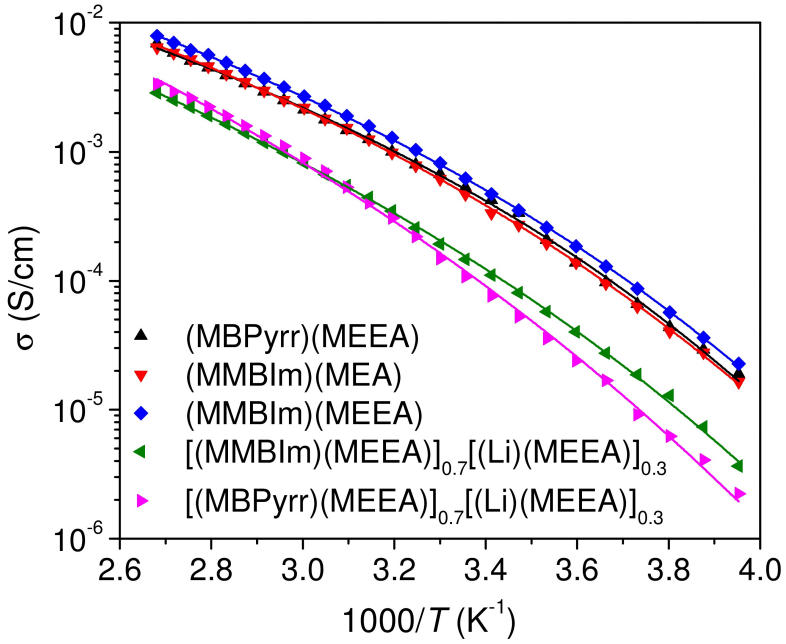

Figure 3. Ionic conductivity as a function of temperature for neat ILs and electrolytes. The solid lines indicate the best fit of data using the VFT equation.

and again suggests that slightly higher energy is required to reach the same ion mobility (Table S1). As expected, the T_0 values in all these systems are about 50 K smaller than the glass transition temperatures T_g and in accordance with the empirical approximation for ionic liquid-based electrolytes: $T_0/T_g \approx 0.75$.[44]

Electrochemical Stability

To evaluate the ESWs, both cathodic and anodic LSV experiments were performed on GC as a working electrode at 20 °C (Figure 4 and Table 1). Relatively wider ESWs are observed for the pyrrolidinium-based ILs with a common anion as compared to the imidazolium-based ILs, but still with narrower ESWs than for phosphonium-based ILs containing the same anion.[10] For the same cation, an increase in the number of ethoxy units in the anions decreases the cathodic stability but the anodic stability significantly increases and thereby an overall wider ESW. For the electrolytes, the pyrrolidinium-based electrolyte has a wider ESW than the imidazolium-based electrolyte. These ESWs (*ca.* 2.8–3.6 V *vs.* Li/Li^+) are narrower than for previously reported ILs and their electrolytes containing non-fluorinated

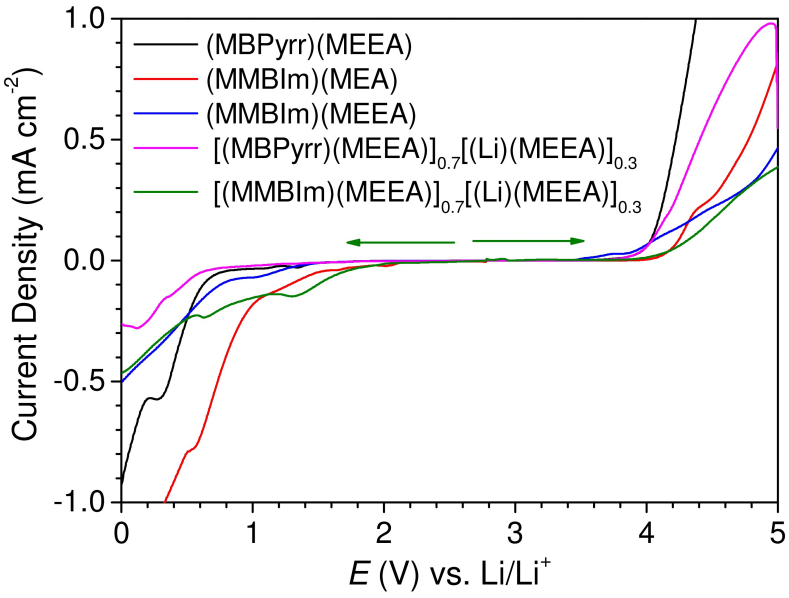

Figure 4. LSV curves of neat ILs and electrolytes on GC electrode at 20 °C.

anions,[45,46] but comparable with conventional LIB electrolytes, such as 1 M $LiPF_6$ in EC:DMC (3.7 V *vs.* Li/Li^+).[47]

The electrochemical stabilities of the electrolytes at different temperatures using a 1 mV s^{-1} scan rate and the long-term reversibility at 30 °C with a 100 mV s^{-1} scan rate are accessed by CV (Figures 5 and 6). The shape of the CV curves remain unaffected by the changes in either the temperature or the scan rate and no additional peaks are observed, indicating the absence of any impurities in these electrolytes.[48] At 30 °C, the imidazolium-based electrolyte shows very stable reversibility in the voltage range from 1.0 to 3.9 V (*vs.* Li/Li^+) but the redox peaks appear at 1.5 and 3.4 V (*vs.* Li/Li^+) at higher temperatures (50 and 80 °C). The reduction peak is attributed to under-potential deposition (UPD) of lithium followed by reduction of the imidazolium cation, while the oxidation peak indicates partial decomposition of the carboxylate anion on the GC electrode.[49,50] Changing the cation from imidazolium to pyrrolidinium, a significantly higher current is produced during the reduction process, while a comparable current is released in the oxidation process, which is accordance to published data.[51] Both the electrolytes revealed excellent long-term electrochemical stability at 30 °C on the surface of a GC electrode (Figure 6). At higher temperature peaks for UPD of lithium are visible at almost the same range as for the imidazolium-based electrolyte. Overall, the pyrrolidinium-based electrolytes exhibit higher electrochemical stabilities than the imidazolium-based electrolytes and vice versa for neat ILs.

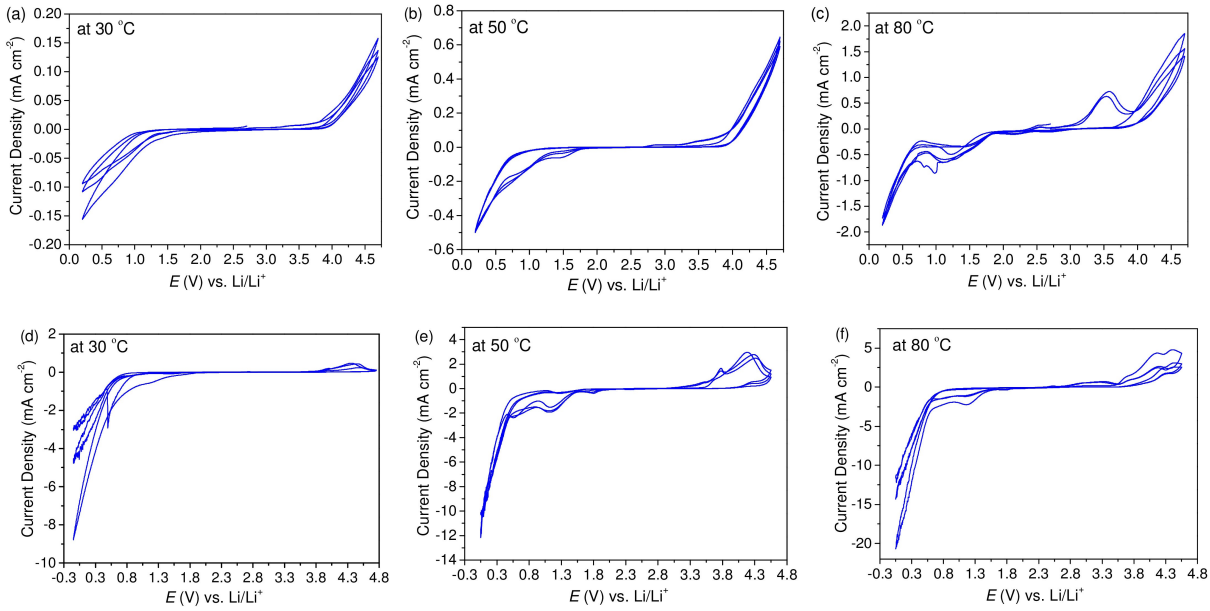

Figure 5. CVs (3 cycles) of the $[(MMBIm)(MEEA)]_{0.7}[(Li)(MEEA)]_{0.3}$ (a–c) and the $[(MBPyrr)(MEEA)]_{0.7}[(Li)(MEEA)]_{0.3}$ (d–f) electrolytes at different temperatures using GC as WE and a scan rate of 1 mV s^{-1}.

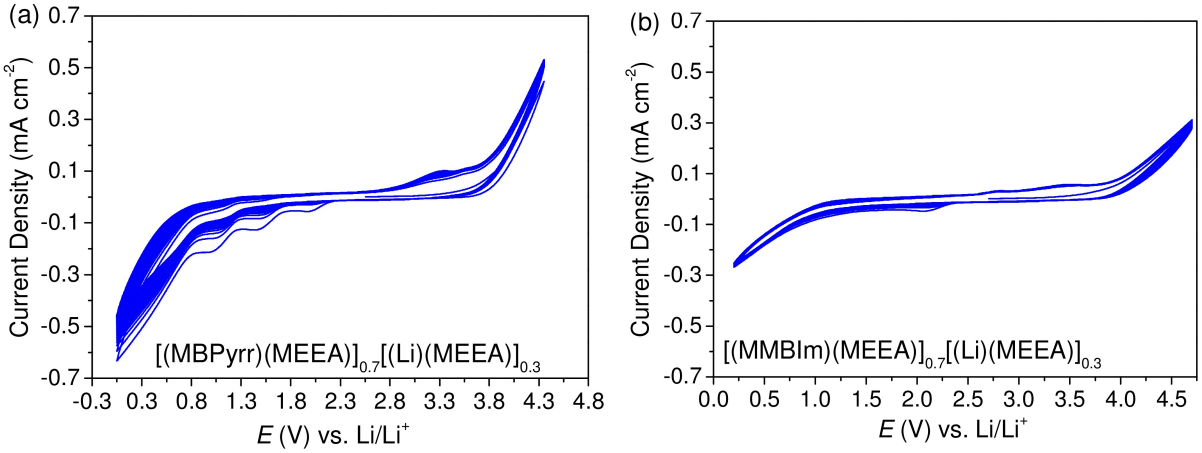

Figure 6. CVs (100 cycles) of the $[(MBPyrr)(MEEA)]_{0.7}[(Li)(MEEA)]_{0.3}$ (a) and $[(MMBIm)(MEEA)]_{0.7}[(Li)(MEEA)]_{0.3}$ (b) electrolytes at 30 °C using GC as WE and a scan rate of 100 mV s^{-1}.

NMR Diffusometry

^{1}H PFG NMR diffusometry was employed to acquire deeper insights into the relative mobility of cations and anions in neat ILs and electrolytes and to better comprehend the transport properties at a molecular level. As expected, the diffusion coefficients of all the ions exhibit a monotonous increase as a function of temperature and follow VFT trends (Figure 7). Similarly to the ionic conductivity data, all the ions in the neat ILs diffuse with comparable diffusion coefficients throughout the studied temperature range (Figure 7a). For the electrolytes, the diffusion coefficients of the all ions in imidazolium-based system are slightly larger than for the pyrrolidinium-based and agree well with the ionic conductivity data. The addition of Li-salt, however, reduces the diffusivity of the MEEA anions in both the electrolytes – although the pyrrolidinium-based electrolyte is affected more due to the dominant electrostatic interactions. Despite its smallest size, the Li^+ ion diffuses the slowest, suggesting strong interactions with the MEEA anions and possible formation of ion-pairs/aggregates (Figure 7b and c). The interactions and aggregates are stronger and bulkier for the pyrrolidinium-based electrolyte, as evident from the slower Li^+ diffusivity (Figure 7d).

The VFT parameters (Eq. (3))[52] of the diffusivity data are larger for the ions of (MMBIm)(MEA) compared to other ILs and even larger for the electrolytes (Table S2), the former can be interpreted as diffusion in a homogeneous matrix, which is essentially governed by the free volume available,[53] while the latter is due to enhanced ion-ion interactions, which is reflected in the slightly higher apparent activation energy, E_D, as well as in D_0. T_0 from ionic conductivity data is lower than T_0 from diffusivity data; the latter is an average of the diffusion coefficients of solitary, ion-paired, and aggregated ions regardless of charge, whereas the former only contains contributions from charged species.[54]

$$D = D_0 \exp\left(\frac{-B}{(T - T_0)}\right) \tag{3}$$

The apparent transference numbers (t_i) for each ion in the electrolytes were calculated from their diffusion coefficients using Eq. (4):[55]

$$t_i = \frac{x_i D_i}{\sum_i x_i D_i} \tag{4}$$

The MEEA anion has higher transference numbers in both electrolytes as compared to the organic cations and the Li^+ cations, and this is obviously due to the higher content of MEEA anions (Figure 8). The t_i of the Li^+ ions is the smallest due to

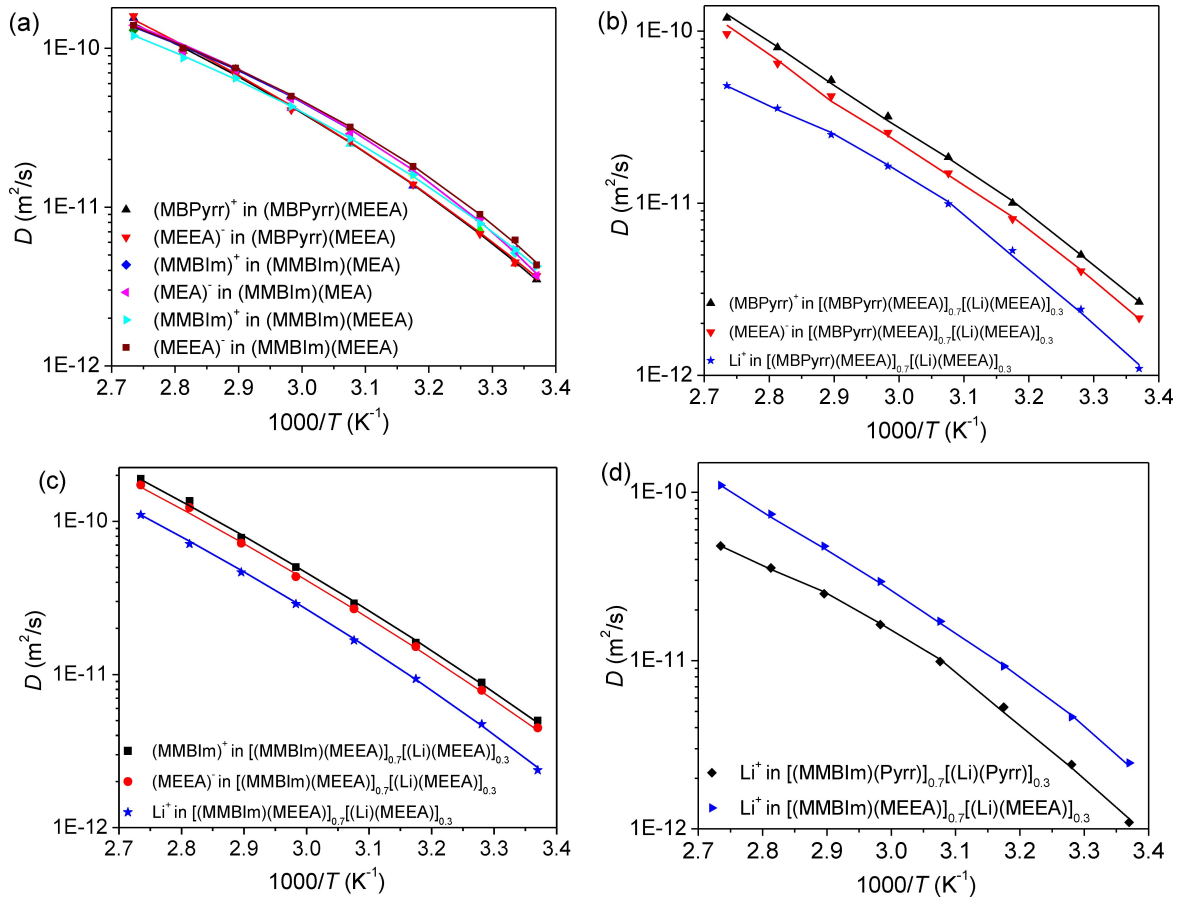

Figure 7. Diffusion coefficients of ions as a function of temperature in the neat ILs (a), $[(Pyrr)(MEEA)]_{0.7}[(Li)(MEEA)]_{0.3}$ electrolyte (b), $[(MMBIm)(MEEA)]_{0.7}[(Li)(MEEA)]_{0.3}$ electrolyte (c), and the comparative Li^+ diffusion in the electrolytes (d).

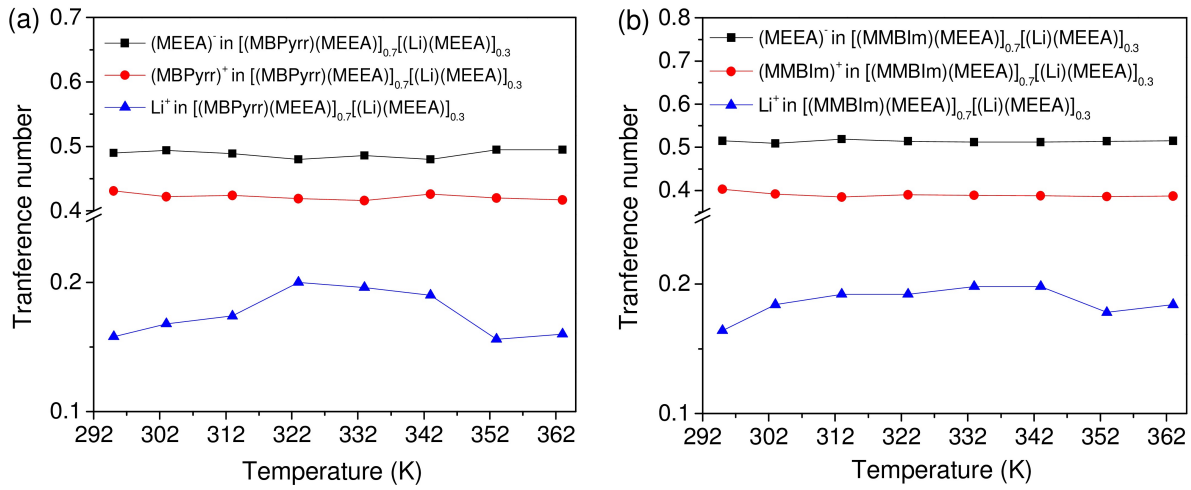

Figure 8. Apparent transfer numbers of ions in the (a) $[(Pyrr)(MEEA)]_{0.7}[(Li)(MEEA)]_{0.3}$ and (b) $[(MMBImd)(MEEA)]_{0.7}[(Li)(MEEA)]_{0.3}$ electrolytes.

two main reasons; the lower concentration and the potential aggregate formation. It is well known that transference numbers calculated from PFG NMR diffusometry are underestimated due to aggregate formation in the electrolytes and do not reflect the true ionic contributions to conductivity, and the values are often approximately half of those determined by electrochemical techniques.[56]

^{7}Li NMR spectroscopy

The full width at half-maximum (fwhm) of the ^{7}Li NMR spectra for the electrolytes initially increase as a function of temperature and then decrease continuously, indicating faster Li^+ ion mobility at slightly elevated temperatures (Figure 9a and Figure S9). This suggests efficient ion dissociation with increasing temperature, leading to homogeneity, which agrees well with the ionic conductivity and ion diffusivity data, and also to our previous study.[18] The chemical environment in the electrolytes is strongly affected by increased temperature, but the electrolytes are influenced differently. The chemical shift of Li^+ in $[(MMBIm)(MEEA)]_{0.7}[(Li)(MEEA)]_{0.3}$ moves towards lower ppms, while for $[(MBPyrr)(MEEA)]_{0.7}[(Li)(MEEA)]_{0.3}$ it shifts towards higher ppms (Figure 9b). This indicates completely different changes in the chemical environments, which also is reflected in the diffusion data (Figure 7d).

Conclusions

Our comparative analysis of pyrrolidinium- and imidazolium-based ILs comprising oligoether anions show the latter to offer slightly better thermal and electrochemical properties, but relatable transport properties. The anions' structural flexibility contributed towards reduced glass transition temperatures of the ILs and the electrolytes. As expected, the ion mobility is reduced upon addition of lithium salts due to reduced free volume and aggregate formation, which also results in lower transference numbers for the Li^+ ions over the whole studied temperature range. The mobility of MEEA anion is strongly affected by addition of the lithium salt, revealing electrostatic interactions between Li^+ ions and anion – aggregate formation

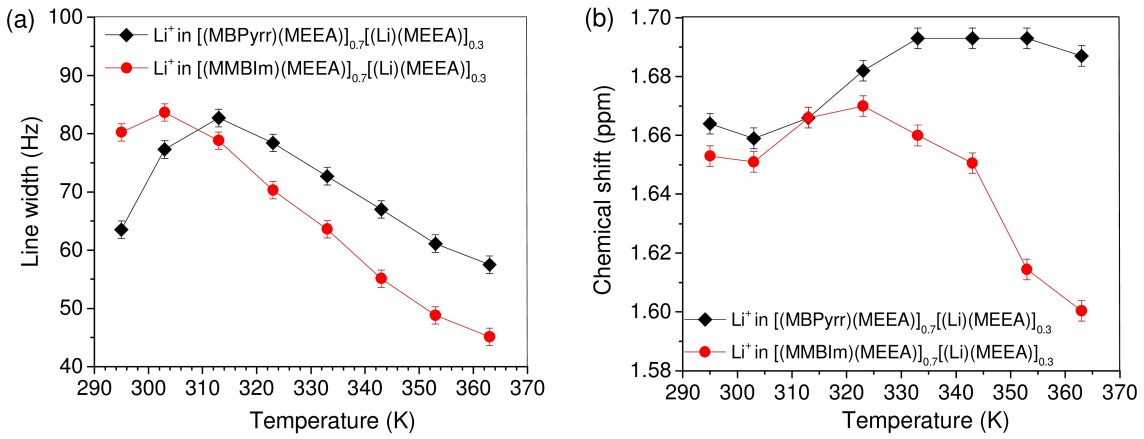

Figure 9. Line widths (a) and chemical shifts (b) of the ^{7}Li NMR spectra for the electrolytes as a function of temperature.

as confirmed by ^{7}Li NMR. Overall, the introduced ILs and the electrolytes can potentially serve as safer electrolytes for 2–3 V batteries, especially operating at elevated temperatures.

Acknowledgements

The financial support from the Swedish Energy Agency (project number: 48194-1) is gratefully acknowledged.

Conflict of Interests

The authors declare no conflict of interest.

Data Availability Statement

The data that support the findings of this study are available in the supplementary material of this article.

Keywords: Fluorine-free ionic liquids · electrolytes · electrochemistry · NMR diffusometry · lithium-ion batteries

[1] M. Smart, B. Ratnakumar, S. Surampudi, *J. Electrochem. Soc.* **1999**, *146* (2), 486.
[2] J. Kalhoff, G. G. Eshetu, D. Bresser, S. Passerini, *ChemSusChem* **2015**, *8* (13), 2154–2175.
[3] Q. Zheng, Y. Yamada, R. Shang, S. Ko, Y.-Y. Lee, K. Kim, E. Nakamura, A. Yamada, *Nat. Energy* **2020**, *5* (4), 291–298.
[4] H. Lee, S. Hwang, M. Kim, K. Kwak, J. Lee, Y.-K. Han, H. Lee, *J. Phys. Chem. Lett.* **2020**, *11* (24), 10382–10387.
[5] K. Deng, Q. Zeng, D. Wang, Z. Liu, G. Wang, Z. Qiu, Y. Zhang, M. Xiao, Y. Meng, *Energy Storage Mater.* **2020**, *32*, 425–447.
[6] F. Larsson, P. Andersson, P. Blomqvist, B.-E. Mellander, *Sci. Rep.* **2017**, *7* (1), 10018.
[7] T. Kawamura, S. Okada, J. I. Yamaki, *J. Power Sources* **2006**, *156* (2), 547–554.
[8] J.-G. Han, M.-Y. Jeong, K. Kim, C. Park, C. H. Sung, D. W. Bak, K. H. Kim, K.-M. Jeong, N.-S. Choi, *J. Power Sources* **2020**, *446*, 227366.
[9] O. E. Bankole, C. Gong, L. Lei, *J. Environment and Ecology* **2013**, *4* (1), 14–28.
[10] F. U. Shah, O. I. Gnezdilov, I. A. Khan, A. Filippov, N. A. Slad, P. Johansson, *J. Phys. Chem. B* **2020**, *124* (43), 9690–9700.
[11] D. Brouillette, G. Perron, J. E. Desnoyers, *J. Solution Chem.* **1998**, *27*, 151–182.
[12] R. Frech, W. Huang, *Macromolecules* **1995**, *28* (4), 1246–1251.
[13] C. A. Angell, Y. Ansari, Z. Zhao, *Faraday Discuss.* **2012**, *154*, 9–27.
[14] K. Ueno, K. Yoshida, M. Tsuchiya, N. Tachikawa, K. Dokko, M. Watanabe, *J. Phys. Chem. B* **2012**, *116* (36), 11323–11331.
[15] S. Fang, G. Wang, L. Qu, D. Luo, L. Yang, S. I. Hirano, *J. Mater. Chem. A* **2015**, *3* (42), 21159–21166.
[16] B. Jache, J. O. Binder, T. Abe, P. Adelhelm, *Phys. Chem. Chem. Phys.* **2016**, *18* (21), 14299–14316.
[17] M. Ahmed, S. Bhowmick, A. Filippov, P. Johansson, F. U. Shah, *Chem. Eur. J.* **2023**, 29, e202301000.
[18] M. Ahmed, S. S. Rao, A. Filippov, P. Johansson, F. U. Shah, *Phys. Chem. Chem. Phys.* **2023**, *25* (4), 3502–3512.
[19] F. U. Shah, O. I. Gnezdilov, R. Gusain, A. Filippov, *Sci. Rep.* **2017**, *7* (1), 16340.
[20] P. M. Bayley, G. H. Lane, N. M. Rocher, B. R. Clare, A. S. Best, D. R. MacFarlane, M. Forsyth, *Phys. Chem. Chem. Phys.* **2009**, *11* (33), 7202–7208.
[21] M. Ghavre, O. Byrne, L. Altes, P. K. Surolia, M. Spulak, B. Quilty, K. R. Thampi, N. Gathergood, *Green Chem.* **2014**, *16* (4), 2252–2265.
[22] L. V. Ganapatibhotla, J. Zheng, D. Roy, S. Krishnan, *Chem. Mater.* **2010**, *22* (23), 6347–6360.
[23] F. Ilyas, M. Ishaq, M. Jabeen, M. Saeed, A. Ihsan, M. Ahmed, *J. Mol. Liq.* **2021**, *343*, 117606.
[24] A. R. Neale, S. Murphy, P. Goodrich, C. Hardacre, J. Jacquemin, *ChemPhysChem* **2017**, *18* (15), 2040–2057.
[25] B. Blümich, *Magn. Reson. Chem.* **1995**, *33* (4), 322–322.
[26] J. E. Tanner, *J. Chem. Phys.* **1970**, (5), 2523–2526.
[27] E. R. Parnham, R. E. Morris, *Chem. Mater.* **2006**, *18* (20), 4882–4887.
[28] J. Sun, D. R. Macfarlane, M. Forsyth, *J. Mater. Chem.* **2001**, *11* (12), 2940–2942.
[29] C. Arbizzani, G. Gabrielli, M. Mastragostino, *J. Power Sources* **2011**, *196* (10), 4801–4805.
[30] M. Kerner, P. Johansson, *Batteries* **2018**, *4* (1), 10.
[31] Y. Cao, T. Mu, *Ind. Eng. Chem. Res.* **2014**, *53* (20), 8651–8664.
[32] Y. Song, L. Liu, X. Zhu, X. Wang, H. Jia, X. Xiao, H. Yu, X. Yang, *Solid State Ionics* **2008**, *179* (13–14), 516–521.
[33] D. R. Macfarlane, S. A. Forsyth, J. Golding, G. Deacon, *Green Chem.* **2002**, *4* (5), 444–448.
[34] S. Fang, Z. Zhang, Y. Jin, L. Yang, S. I. Hirano, K. Tachibana, S. Katayama, *J. Power Sources* **2011**, *196* (13), 5637–5644.
[35] F. U. Shah, S. Glavatskih, P. M. Dean, D. R. MacFarlane, M. Forsyth, O. N. Antzutkin, *J. Mater. Chem.* **2012**, *22* (14), 6928–6938.
[36] Z. B. Zhou, H. Matsumoto, K. Tatsumi, *Chem. Eur. J.* **2005**, *11* (2), 752–766.
[37] Z. B. Zhou, H. Matsumoto, K. Tatsumi, *Chem. Eur. J.* **2004**, *10* (24), 6581–6591.
[38] S. Bhowmick, A. Filippov, I. A. Khan, F. U. Shah, *Phys. Chem. Chem. Phys.* **2022**, *24* (38), 23289–23300.
[39] I. A. Khan, O. I. Gnezdilov, A. Filippov, F. U. Shah, *ACS Sustainable Chem. Eng.* **2021**, *9* (23), 7769–7780.
[40] C. R. Pope, M. Kar, D. R. MacFarlane, M. Armand, M. Forsyth, L. A. O'Dell, *ChemPhysChem* **2016**, *17* (20), 3187–3195.
[41] S. Ferrari, E. Quartarone, P. Mustarelli, A. Magistris, M. Fagnoni, S. Protti, C. Gerbaldi, A. Spinella, *J. Power Sources* **2010**, *195* (2), 559–566.
[42] C. Schreiner, S. Zugmann, R. Hartl, H. J. Gores, *J. Chem. Eng. Data* **2010**, *55* (5), 1784–1788.
[43] F. Stickel, E. W. Fischer, R. Richert, *J. Chem. Phys.* **1996**, *104* (5), 2043–2055.
[44] M. Galiński, A. Lewandowski, I. Stępniak, *Electrochim. Acta* **2006**, *51* (26), 5567–5580.
[45] I. A. Khan, Y.-L. Wang, F. U. Shah, *J. Energy Chem.* **2022**, *69*, 174–184.
[46] N. Karimi, M. Zarrabeitia, A. Mariani, D. Gatti, A. Varzi, S. Passerini, *Adv. Energy Mater.* **2021**, *11* (4), 2003521.
[47] J. B. Goodenough, Y. Kim, *Chem. Mater.* **2010**, *22* (3), 587–603.
[48] H. Liu, H. Yu, *J. Mater. Sci. Technol.* **2019**, *35* (4), 674–686.
[49] R. Wibowo, S. E. W. Jones, R. G. Compton, *J. Chem. Eng. Data* **2010**, *55* (3), 1374–1376.
[50] L. Gasparotto, N. Borisenko, N. Bocchi, S. Z. El Abedin, F. Endres, *Phys. Chem. Chem. Phys.* **2009**, *11* (47), 11140–11145.
[51] X.-G. Sun, S. Dai, *Electrochim. Acta* **2010**, *55* (15), 4618–4626.
[52] A. Noda, K. Hayamizu, M, Watanabe, *J. Phys. Chem. B* **2001**, *105*, 4603–4610.
[53] A. Filippov, B. Munavirov, S. Glavatskih, F. U. Shah, O. N. Antzutkin, *Front. Chem.* **2020**, *8*, 119.
[54] A. K. Sethurajan, S. A. Krachkovskiy, I. C. Halalay, G. R. Goward, B. Protas, *J. Phys. Chem. B* **2015**, *119* (37), 12238–12248.
[55] T. Fromling, M. Kunze, M. Schonhoff, J. Sundermeyer, B. Roling, *J. Phys. Chem. B* **2008**, *112* (41), 12985–12990.
[56] M. Gouverneur, J. Kopp, L. Van Wüllen, M. Schönhoff, *Phys. Chem. Chem. Phys.* **2015**, *17* (45), 30680–30686.

Manuscript received: October 31, 2023
Revised manuscript received: February 12, 2024
Accepted manuscript online: February 13, 2024
Version of record online: ■■, ■■

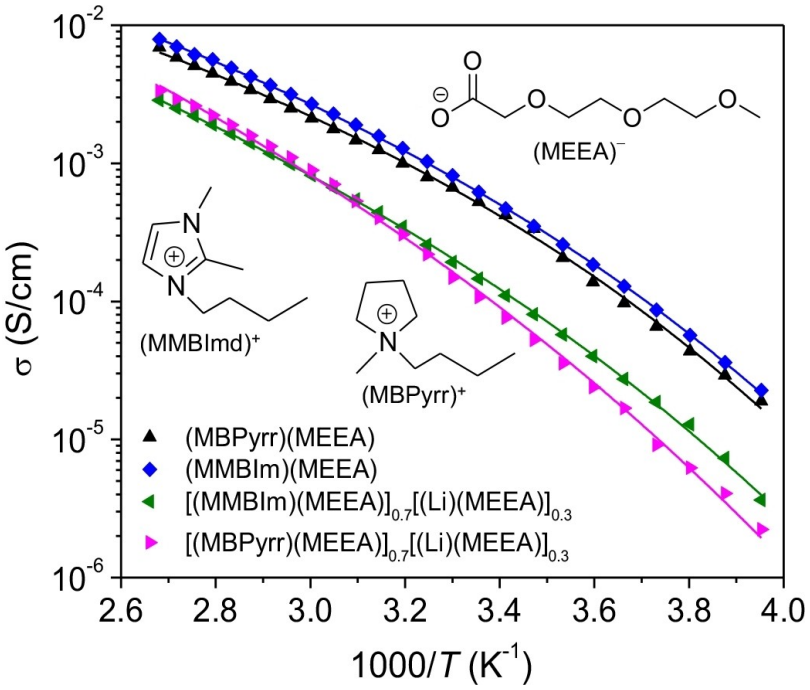

M. Ahmed, A. Filippov, P. Johansson, F. U. Shah**

Here we present fluorine-free pyrrolidinium- and imidazolium-based ionic liquids and electrolytes with flexible oligoether anions. The electrolytes offer promising physicochemical and transport properties that can potentially be used in lithium batteries, especially at elevated temperatures.